Research Square

Preprints are preliminary reports that have not undergone peer review.
They should not be considered conclusive, used to inform clinical practice,
or referenced by the media as validated information.

Influence of river routing resolution and parameterization on ocean circulation and sea surface temperature in seasonal prediction system

Suryun Ham

suryun01@gmail.com

APEC Climate Center https://orcid.org/0000-0002-7354-3968

Johan Lee

National Institute of Meteorological Sciences

Beomcheol Shin

National Institute of Meteorological Sciences

Research Article

Keywords:

Posted Date: November 2nd, 2026

DOI: https://doi.org/10.21203/rs.3.rs-10876204/v1

License: This work is licensed under a Creative Commons Attribution 4.0 International License.
Read Full License

Influence of river routing resolution and parameterization on ocean circulation and sea surface temperature in seasonal prediction system

Suryun Ham[1*], Johan Lee[2], and Beomcheol Shin[2]

[1]Climate Services and Research Division, APEC Climate Center, Korea
[2]Climate Research Department, National Institute of Meteorological Sciences, Korea

(To be submitted Climate dynamics)

August 2026

*Corresponding author address:
Suryun Ham, Climate Services and Research Department,
APEC Climate Center, Busan, 48058, Korea
E-mail: suryun01@gmail.com

Abstract

River discharge represents an important freshwater forcing in coupled climate systems, yet the river routing components used in operational seasonal prediction systems often remain at substantially coarser spatial resolutions than their atmospheric, land, and ocean model components. This study investigates the influence of river routing resolution and associated parameterization on ocean simulation in the Korea Meteorological Administration (KMA) Global Seasonal Forecasting System version 6 (GloSea6). The TRIP river routing model, originally hard-coded at a fixed 1° resolution, was modified to accommodate flexible spatial resolutions, and a higher-resolution configuration of 0.5° was implemented using refined river direction, flow sequence, and river-mouth information.

Increasing the river routing resolution provides a more detailed representation of river networks and river mouths, leading to changes in freshwater discharge and coastal salinity. These changes modify upper-ocean stratification and circulation, reducing regional SST biases around the Korean Peninsula, Japan, and the Sea of Okhotsk. Although salinity changes are relatively limited over the open ocean, associated adjustments in mixed layer depth, circulation, and SST extend into parts of the tropical Pacific and Indian Oceans. These results demonstrate that river routing representation constitutes a non-negligible source of freshwater forcing uncertainty in coupled seasonal prediction systems. While increasing routing resolution alone is insufficient to eliminate systematic ocean biases, improved representation of river networks and appropriate parameter optimization can influence ocean salinity, stratification, circulation, and SST from coastal to broader oceanic scales. The results therefore emphasize the importance of

a more physically realistic treatment of river routing and freshwater discharge for improving ocean simulations in future coupled seasonal prediction systems.

Key words: River routing, Freshwater forcing, Seasonal prediction, Ocean circulation

1. Introduction

Hydrological models are important tools for flood and drought management and preparedness and are widely used in climate projection. Gudmundsson et al. (2021) showed that observed changes in river flow are consistent with climatic changes, while Sauer et al. (2021) identified a climate signal in trends in flood-related damages. Advances in computational capabilities have facilitated the development of increasingly sophisticated hydrological models capable of representing complex river-channel processes. For example, the Copernicus Global Flood Awareness System (Alfieri et al., 2013) employs a coupled land surface scheme and river routing model to generate operational forecasts at daily time steps and a horizontal resolution of 0.1°. This system routes runoff generated by the land surface scheme through the river network and calculates groundwater fluxes (Burek et al. 2013; Hirpa et al. 2018). The freshwater routed through such river systems is, however, not solely a terrestrial concern. Large rivers deliver their discharge to shelf seas as buoyant plumes that can extend hundreds of kilometers from the river mouth, and extreme upstream flooding can release freshwater pulses far exceeding the seasonal norm, as observed during the record Changjiang (Yangtze River) flood of summer 2020 (Lee et al. 2025), with consequences for coastal circulation, ecosystems, and fisheries.

Freshwater inflow into the ocean directly affects upper-ocean salinity and stratification. The resulting salinity-induced stratification can promote the formation of a barrier layer between the surface mixed layer and the thermocline, thereby suppressing vertical mixing and reducing the entrainment of colder subsurface water into the surface layer (Park et al. 2011). Consequently, variations in freshwater flux can alter salinity, mixed layer depth, ocean circulation, and sea surface temperature (SST), potentially

affecting air-sea interactions and providing feedback to the atmosphere (e.g., Zhang et al., 2011; Ham et al. 2012; Kako et al. 2016). For example, Howden and Murtugudde (2001) showed that freshwater forcing can decrease surface temperature through enhanced entrainment cooling. Ham et al. (2012) showed that the inclusion of river routing reduces coastal salinity and mixed layer depth, leading to weaker trade winds and reduced vertical mixing in the tropical Pacific and an associated increase in SST. In contrast, Masson and Delecluse (2001) demonstrated that river runoff did not exert a clear influence on SST in their ocean model experiments. Despite the recognized influence of freshwater flux on SST and atmospheric circulation, the effects of river routing on coupled climate simulations remains relatively understudied. This may partly reflect the fact that land-surface and riverine processes have traditionally been considered to exert predominantly local or regional influences, whereas climate-model development has often focused on processes affecting the large-scale climate system. Nevertheless, recent advances in global hydrological modeling and coupled Earth system modeling have highlighted the potential importance of more realistically representing river discharge and freshwater forcing.

Advances in global hydrological modeling have also led to the development and widespread use of global runoff and river discharge datasets. In parallel, increasingly sophisticated global river-routing models have been developed and coupled with land surface models, facilitating their application within climate modeling systems. For example, Nitta et al. (2020) developed the Integrated Land Simulator (ILS), which couples the Minimal Advanced Treatments of Surface Interaction and Runoff (MATSIRO) land surface model with the Catchment-based Macro-scale Floodplain (CaMa-Flood) hydrodynamic model to provide an integrated framework for land and river simulation.

Li et al. (2024) further evaluated river discharge simulated by an offline coupling of the Community Land Model (CLM) and CaMa-Flood under different meteorological forcing datasets. These developments provide a foundation for improving the representation of river processes in coupled climate models.

These advances have also motivated the improved representation of river routing and freshwater discharge in operational coupled prediction systems. For example, an earlier version of the European Centre for Medium-Range Weather Forecast (ECMWF) Integrated Forecasting System (IFS) was coupled with the Total Runoff Integrating Pathways 2 (TRIP2; Ngo-Duc et al. 2007) river-routing model (Pappenberger et al. 2010). More recently, the more sophisticated CaMa-Flood river-routing model has been integrated into the ECMWF land surface system to improve the representation of river dynamics and terrestrial freshwater processes (Boussetta et al. 2021). Similarly, Woldemeskel et al. (2025) coupled the JULES land surface model with CaMa-Flood and evaluated its ability to simulate streamflow across Australia, demonstrating its potential for operational hydrological forecasting. These developments highlight the increasing integration of advanced river-routing schemes into large-scale land and hydrological modeling systems.

Operational forecasting centers worldwide have continuously developed coupled climate prediction systems to improve seasonal prediction skill. The Korea Meteorological Administration (KMA) has operated a dynamical long-range prediction system since 1999. Since 2010, KMA has employed a fully coupled atmosphere-land-ocean-sea-ice seasonal prediction system based initially on the Global Seasonal Forecasting System version 4 (GloSea4) developed by the UK Met Office. The current operational system, GloSea6, incorporates improved physical parameterizations and

higher spatial resolution compared with its predecessors, GloSea4 and GloSea5 (MacLachlan et al. 2015; Walters et al. 2017; Ham et al. 2024).

GloSea6 employs the Total Runoff Integrating Pathways (TRIP; Oki and Sud 1998) model, which uses a simplified advection scheme (Oki 1997) to route total runoff along prescribed river channels at a fixed horizontal resolution of $1^{\circ}\times1^{\circ}$ with a 3-h time step. Land surface runoff accumulated over this time step is first mapped onto the river grid before the TRIP calculation. After routing, soil moisture increments and total outflow at river mouths are remapped back to the atmosphere grid (Falloon and Betts 2006; Walters et al. 2017). During the early implementation of TRIP, atmospheric and land surface models typically operated at N96 (~135 km) or coarser resolutions, for which the 1° resolution of TRIP was broadly comparable. However, as atmospheric and land components have moved toward substantially higher spatial resolutions (e.g. N216; ~60 km), the coarse resolution of TRIP has introduced an increasing spatial-scale mismatch among model components, potentially limiting the realistic representation of river routing and freshwater discharge. Although implementing a more sophisticated and physically comprehensive river routing model, such as CaMa-Flood, would ultimately be desirable, this study takes an intermediate step by examining the impact of increasing the spatial resolution of the existing TRIP model.

In this study, the river routing modules within the operational KMA GloSea6 system were modified to accommodate spatial resolutions beyond the default fixed 1° configuration. A 0.5° TRIP configuration was implemented to investigate how increased river routing resolution affects freshwater discharge and the associated ocean response in a coupled seasonal prediction system. In addition, sensitivity experiments with resolution-dependent routing parameters were conducted to distinguish the effects of spatial

resolution from those of parameter optimization. Particular attention is given to changes in salinity, upper-ocean stratification, ocean circulation, and SST over East Asia and the tropical Indo-Pacific. By comparing experiments with unchanged and resolution-optimized routing parameters, we further distinguish the direct effect of increased river-routing resolution from that associated with parameter recalibration.

The remainder of this paper is organized as follows. Section 2 describes the KMA operational system and the experimental configurations with increased river routing resolution. Section 3 examines the impacts of increased river routing resolution on the coupled seasonal prediction system, and Section 4 summarizes the major findings and conclusions.

2. Models and experimental design

In this study, seasonal hindcast datasets produced by the KMA operational prediction system were analyzed. KMA operates a seasonal prediction system developed in collaboration with the UK Met Office. The system was initially based on GloSea4, was subsequently upgraded to GloSea5, and has operated with GloSea6 since 2021. Here, GloSea6 is used to investigate the effects of river-routing processes within a coupled seasonal prediction system. GloSea6 is a fully coupled global climate prediction system consisting of atmosphere (Unified Model; UM), ocean (Nucleus for European Modeling of the Ocean; NEMO), land surface (Joint UK Land Environment Simulator; JULES) and sea-ice (Los Alamos sea ice model; CICE) components coupled through OASIS (MacLachlan et al. 2015). The atmospheric component uses an N216L85 configuration with a horizontal resolution of approximately 60 km, while the ocean component uses the ORCA0.25L75 configuration with a nominal horizontal resolution of 0.25° on a tripolar

grid. The Stochastic Kinetic Energy Backscatter scheme version 2 (SKEB2; Tennant et al. 2011) and the Stochastic Perturbation of Tendencies scheme (SPT; Sanchez et al. 2016) are used to generate ensemble spread among members initialized from the same analysis. Since 2021, KMA has operated GloSea6 based on the Global Coupled configuration 3.2 (GC3.2), replacing the previous GloSea5 system based on GC2.0 (Williams et al. 2015). Further details of GloSea5 and GloSea6 configurations are provided in MacLachlan et al. (2015), Williams et al. (2015), and Kettleborough et al. (2025).

The GloSea6 employs the Total Runoff Integrating Pathways(TRIP; Oki and Sud 1998) model, which uses a simplified advection approach (Oki 1997) to route total runoff along prescribed river channels at a fixed horizontal resolution of $1^{\circ}\times1^{\circ}$ with a 3-h time step. TRIP represents each river grid cell as a simple reservoir, with surface runoff (Q_{in}) as input and river discharge (Q_{out}) as output. The change in river storage (S) in the reservoir can be expressed as follows:

$$\frac{dS}{dt} = Q_{in} - Q_{out};\ Q_{out} = \frac{v}{\tau d}S$$

where v [m s^{-1}] is the effective velocity, d [m] is the river length, τ [dimensionless] is the meandering factor representing river curvature, S [kg m^{-2}] is the river storage, and Q [kg m^{-2} s^{-1}] denotes river discharge. Figure 1 illustrates the model structure and spatial resolution of GloSea6, highlighting the input and output variables associated with the TRIP river routing model. River flow is calculated from runoff generated by the land surface component, and the resulting freshwater discharge at river mouths is passed to the ocean model. To simulate river flow, the TRIP model requires four input datasets: initial river water storage, river flow direction, river sequence information, and a river-number dataset defining river-mouth locations for coupling with the ocean model. These datasets

are defined on a global grid and used internally by the TRIP model. In the original GloSea5 implementation, the TRIP modules are coupled to the land-surface model and hard-coded to operate at a fixed 1° resolution using predefined ancillary data.

Recently, Kim et al. (2025) investigated the impacts of increasing the spatial resolution of TRIP within the JULES land-surface model from 1° to 0.5° and 0.125°, and optimized the associated routing parameters, including flow velocity and the meandering coefficient. Their results showed that increasing river-model resolution improved the representation of river networks and discharge dynamics while also highlighting the importance of appropriate parameter calibration, particularly for flow velocity and meandering coefficients. In this study, the high-resolution (0.5° and 0.125°) river direction and sequential datasets used in Kim et al. (2025) are introduced into the GloSea6-TRIP system, which originally operated at a fixed 1° resolution, in order to investigate effects of increased river-routing resolution within a coupled seasonal prediction system. The river-direction and river-sequence datasets were converted into ancillary files compatible with the GloSea6 input format. In addition, a new river-number dataset was generated to define river-mouth locations for coupling with the ocean model.

In conjunction with this, the hard-coded modules of TRIP were modified and further developed to enable the application of flexible spatial resolution. In the original code, grid-cell areas were computed using predefined latitude-dependent values from an ASCII file based on a fixed 1° grid. This approach was replaced by a dynamic calculation of grid-cell areas based directly on the actual latitude and longitude coordinates. In the original 1° configuration, latitude and longitude values were represented as integers, allowing array indices and geographical coordinates to be interchangeably in the calculations. To support higher-resolution TRIP configurations, latitude and longitude values were treated

as real values instead of integer values, and all modules were revised to decouple array indices from latitude and longitude values, thereby removing the resolution-dependent constraints of the original implementation. As a result, the TRIP model was configured to operate with ancillary data at various spatial resolutions, allowing it to flexibly adapt to the resolution of the input datasets.

The experiment in which the TRIP model within GloSea6 is configured at a 1° resolution, consistent with the existing operational seasonal prediction system, is referred to as OPER. The experiment using a 0.5° TRIP configuration, with twice the horizontal resolution of OPER, is referred to as HALF. As the spatial resolution increases, river channels that were previously represented within a single grid cell are distributed across multiple grid cells, effectively increasing the represented river length. This change requires recalibration of routing parameters, particularly flow velocity and the meandering coefficients, to maintain realistic river-flow characteristics. Accordingly, an additional 0.5° experiment using flow velocity and meandering parameters optimized for this resolution following Kim et al. (2025) is referred to as HALFv. In OPER and HALF, the river-flow velocity and meandering coefficients are set to 0.4 and 1.4, respectively, whereas the corresponding values in HALFv are 0.5 and 0.525. Although an additional experiment (EIGHTH) with a 0.125° river-routing resolution, finer than the atmospheric resolution, was initially implemented, it was excluded from the subsequent analysis because it produced unrealistically low river-storage values. This behavior likely reflects the strong sensitivity of river storage to routing parameters when the channel length and grid geometry are substantially altered at very high resolution.

Figure 2 shows the spatial distribution of the GloSea6 ancillary (input) datasets used to drive the river routing component over the East Asia region. River directions (Fig. 2a,

d) are encoded as integers from 0 to 9, with each code specifying the direction of downstream flow. In these datasets, 0 denotes a river origin, and 9 denotes an river outlet to the ocean. The river-sequence fields (Fig. 2b, e) define the routing order used for upstream-to-downstream accumulation during channel flow computation. The river-number maps (Fig. 2c, f) are used to define river discharge outlets and to provide the corresponding freshwater flux information for coupling to the ocean model. At higher spatial resolution, river-flow pathways are represented in greater detail, and river-mouth locations that were previously distributed over relatively broad areas become more spatially confined. Apart from slight shifts toward the land-sea mask boundary associated with the finer grid, however, the underlying river-number assignments remain largely unchanged.

To assess the influence of river routing on seasonal forecasts, boreal summer simulations were analyzed for the five-year period 1997-2001, when river discharge is relatively pronounced over East Asia. Simulations were initialized on 1, 9, 17, and 25 May, with three perturbed ensemble members for each initialization date. This design yielded 60 hindcast realizations for each experiment (5 years × 4 initialization dates × 3 ensemble members). Three-month forecasts for June-August (JJA) were then analyzed using the ensemble mean. To evaluate model biases, the fifth generation ECMWF atmospheric reanalysis (ERA5; Hersbach et al. 2020) and Ocean Reanalysis System 5 (ORAS5; Zuo et al. 2019) were used for atmospheric and ocean variables, respectively.

3. Impact of increased river routing resolution

a. East Asia

Figure 3 shows spatial distributions of simulated river water storage and river outflow

over East Asia in the OPER, HALF, and HALFv experiments. Increasing the river-routing resolution from 1° to 0.5° results in a more spatially detailed distribution of river water storage, with finer gradients and clearer delineation of major river basins. Similarly, river outflow in HALF and HALFv is more spatially confined along major river channels, such as the Yangtze and Amur Rivers, and their coastal outlets than in OPER. River outflow becomes more concentrated within major river basins, whereas distinct changes are also evident in regions with few or no defined river channels. In HALFv, which incorporates optimized routing parameters, river storage becomes further confined to major river channels compared with HALF.

Figure 4 shows the surface runoff bias in OPER relative to ERA5 and the differences in surface runoff between the higher-resolution experiments and OPER. In OPER, surface runoff exhibits pronounced regional biases over East Asia, with both positive and negative anomalies relative to ERA5. Relatively large biases occur over several coastal regions, major river basins, and high-latitude areas. Surface runoff in HALF exhibits clear spatial deviations in runoff compared to the OPER experiment. In HALFv, surface runoff decreases along coastal regions near 40N° relative to OPER, whereas increases occur along the southeastern coast of China. These results indicate that changes in the river-routing configuration are accompanied by regional changes in simulated surface runoff, particularly near coastal regions and major drainage basins. Such changes may reflect coupled land-atmosphere feedbacks associated with the modified freshwater routing.

Changes in river discharge directly modify the ocean salinity distribution through variations in freshwater input to the ocean. Figure 5 shows the sea surface salinity bias in OPER and the corresponding differences in HALF and HALFv. In OPER, pronounced salinity biases occur in river-influenced coastal regions, particularly in the East China Sea

and adjacent marginal seas. Many of these biases are located near major river mouths, suggesting a potential contribution from the representation of riverine freshwater input. Relative to OPER, HALF shows pronounced regional changes in salinity, particularly near river mouths and along coastal current pathways. These differences indicate that increased routing resolution modifies the spatial distribution of freshwater discharge, and consequently affects coastal salinity. Additional salinity changes occur in HALFv, in which resolution-optimized flow velocity and meandering parameters are applied. Notably, the positive salinity bias along the coast of the Sea of Okhotsk near the mouth of the Amur River is substantially reduced in HALF and HALFv, consistent with the better-resolved river-mouth locations and redistribution of freshwater input at higher routing resolution. Salinity biases along the Korean Peninsula and Japanese coasts are also reduced in the higher-resolution experiments, coinciding with changes in the representation of nearby river-mouth locations. In contrast, the negative salinity bias near the Yangtze River mouth becomes more pronounced. Because TRIP does not explicitly represent dam and reservoir regulation, the absence of these processes may contribute to the persistent bias in this heavily regulated river basin.

Freshwater-induced changes in ocean salinity can modify upper-ocean stratification and thereby affect SST. Figure 6 shows pronounced SST biases in OPER over the marginal seas of East Asia, particularly in the Sea of Okhotsk and along the coastal regions of Japan and East China Sea. Several of these SST biases spatially coincide with the sea surface salinity biases shown in Fig. 5, suggesting a possible contribution from biases in freshwater forcing and the associated upper-ocean salinity structure. At higher river-routing resolution, SST biases are reduced in several regions that also exhibit substantial salinity changes, most notably in the Sea of Okhotsk. In contrast, SST

increases over the Kuroshio Extension region east of Japan, thereby amplifying the existing warm bias. HALFv produces additional SST changes in the Sea of Okhotsk and east of Japan relative to HALF, indicating sensitivity of upper-ocean thermal response to the routing parameters.

To examine the ocean-circulation changes associated with the salinity response, Fig. 7 shows sea surface height and surface wind stress over the East Asian marginal seas. The ORAS5 captures the major circulation features around East Asian, including the northward-flowing Kuroshio and its eastward extension south of Japan, together with circulation in the marginal seas. In OPER, the southward cold-current flow from southern Sea of Okhotsk toward the East Sea along the Korean Peninsula is overestimated, while the characteristic meandering structure associated with Kuroshio is not well reproduced. In addition, pronounced northwestward biases extend from the seas surrounding the Korean Peninsula toward the South China Sea. In the higher-resolution river routing experiments, the pronounced northwestward bias over the East Sea is substantially reduced, particularly in HALFv. However, the southeasterly surface wind stress component over the Yellow Sea becomes stronger in the higher-resolution experiments.

During boreal summer, ocean circulation around East Asia is strongly influenced by the Kuroshio, which branches from the westward-flowing North Equatorial Current east of the Philippines and flows northward along the western boundary of the North Pacific. Kuroshio-derived waters contribute to the Yellow Sea Warm Current and the Tsushima Warm Current, while the main Kuroshio flows northeastward south of Japan before extending eastward into the North Pacific. Meanwhile, the Liman Cold Current flows southward along the continental margin, contributing to the southward cold-water pathway associated with the North Korean Cold Current in the East Sea.

Changes in freshwater input modify salinity and upper-ocean density structure, potentially affecting both ocean circulation and temperature. In the higher-resolution experiments, the negative salinity bias near the Yangtze River mouth becomes stronger, whereas positive salinity bias near the Han River in Korea and the Yellow River in China are reduced. The associated salinity and circulation changes may favor greater northward intrusion of relatively warm water into the Yellow Sea, consistent with the slight SST increase in this region. In the Sea of Okhotsk, the positive salinity bias in OPER is reduced in the higher-resolution experiments, consistent with increased freshwater influence. The resulting fresher surface conditions are expected to enhance upper-ocean stratification, which may contribute to the simulated SST increase. The higher-resolution experiments also show a weakening of the excessive southward cold-current influence toward the East Sea, accompanied by a reduction in the cold SST bias, particularly in HALFv. These results suggest that the freshwater-induced salinity changes are associated with adjustments in both upper-ocean stratification and regional circulation, contributing to the SST response over the East Asian marginal seas.

b. Tropics

Although the salinity response to changes in river routing is primarily concentrated in coastal regions, associated oceanic adjustments may extend beyond the immediate vicinity of river mouths through changes in circulation. Therefore, we examine whether changes in the river routing configuration are accompanied by broader oceanic responses in the tropical Pacific and Indian Oceans.

Figure 8 shows the salinity biases in OPER across low to mid-latitudes, with the salinity differences resulting from changes in river routing model resolution. Changes in

384 salinity associated with modifications to river routing resolution are limited over the open
385 ocean and remain relatively small outside coastal regions. However, noticeable changes
386 are shown in coastal areas and over the Maritime Continent. Although the changes over
387 the open ocean are relatively small, we further investigate how freshwater variations in
388 coastal regions are associated with changes in ocean circulation.

389 Figure 9 shows the mixed layer depth and upper-ocean current distributions over the
390 tropical Indo-Pacific. The spatial distribution of mixed layer depth broadly coincides with
391 major tropical current systems, reflecting coupled effects of surface forcing, stratification,
392 and ocean dynamics. Compared with ORAS5, OPER simulates an excessively strong
393 Equatorial Countercurrent and weaker North and South Equatorial Currents. These
394 circulation biases are accompanied by excessively shallow mixed layer depths in regions
395 dominated by the North and South Equatorial Currents. HALF reduces the excessive
396 Equatorial Countercurrent bias found in OPER, together with partial reductions in mixed
397 layer depth biases along the North Pacific current pathways. However, mixed layer depth
398 biases increase in some regions of the Southern Hemisphere and Indian Ocean. The
399 HALFv experiment shows more widespread improvement in mixed layer depth,
400 particularly south of the equator, over the Indian Ocean, and along the western Pacific
401 and the North Equatorial Current regions.

402 Figure 10 extends the SST analysis beyond the East Asian marginal seas. OPER
403 exhibits a cold bias around the Korean Peninsula and pronounced warm biases along the
404 Kuroshio and California Current regions. Additionally, a weak cold bias appears over the
405 Maritime Continent, while a weak warm bias is present in parts of the Indian Ocean. In
406 HALF, SST increases in regions where cold biases are present in OPER, such as around
407 the Korean Peninsula and the Maritime Continent, whereas a reduction in SST is evident

over the North Pacific near 20°N. However, over parts of the North Pacific, the SST response in HALF overcompensates for the OPER bias, resulting in biases of the opposite sign. Notably, HALFv exhibits a substantial reduction in biases compared to the OPER over the North Pacific, especially in the California Current region, as well as clear improvements over the Indian Ocean and tropical eastern Pacific.

Figure 11 shows the vertical temperature structure averaged over the tropical region (5°S-5°N). Relative to OPER, HALF exhibits pronounced temperature biases extending from the surface to the subsurface ocean, particularly over the Pacific and Indian Ocean. Relative to OPER, HALF produces relatively modest changes in the vertical temperature structure, whereas HALFv shows more pronounced subsurface temperature changes, particularly in the Indian Ocean. These results suggest that the optimized river-routing parameters can influence not only surface conditions but also the subsurface thermal structure of the tropical oceans. This response is consistent with the changes in mixed layer depth and ocean circulation shown above. Overall, however, increasing river-routing resolution alone produces only limited and regionally inconsistent reductions in ocean circulation and temperature biases. Appropriate recalibration of routing parameters is therefore critical when river-routing resolution is changed.

4. Concluding remarks

This study investigated the impact of enhancing the spatial resolution of the river routing model on seasonal predictions using the KMA GloSea6 operational system. The TRIP river routing model in GloSea6, originally hard-coded at a fixed 1° resolution, was modified to accommodate ancillary datasets at flexible spatial resolutions, and a higher resolution configuration of 0.5° was implemented. Sensitivity experiments were

conducted to separately examine the effects of increased routing resolution and the optimization of key routing parameters, including river flow velocity and meandering coefficients. The resulting changes in freshwater discharge and their impacts on ocean salinity, circulation, and temperature were evaluated over East Asia and the broader tropical Indo-Pacific region. Through these experiments, we aimed to assess whether improving the representation of river routing can contribute to reducing systematic ocean biases in an operational coupled seasonal prediction system.

Increasing the TRIP resolution from 1° to 0.5° produced a more detailed representation of river networks and river-mouth locations, resulting in substantial changes in the spatial distribution of river storage and freshwater discharge. These changes directly modified coastal salinity and subsequently affected upper-ocean stratification, circulation, and SST, with notable improvements around the Korean Peninsula, Japan, and the Sea of Okhotsk; in particular, the excessive cold-current influence and associated cold SST bias in the East Sea were reduced. Although the influence of routing resolution on open-ocean salinity was relatively limited, circulation and mixed-layer responses extended into the tropical Pacific and Indian Oceans, indicating that the effects of modified coastal freshwater forcing are not necessarily confined to river-mouth regions. Increasing resolution alone, however, did not consistently reduce ocean biases, and some errors were amplified in regions such as the North Pacific. In contrast, the HALFv experiment, which combined the 0.5° resolution with optimized flow velocity and meandering parameters, generally showed more substantial improvements, including reduced SST and mixed layer depth biases in parts of the North Pacific, California Current region, western Pacific, and Indian Ocean.

Overall, increasing the spatial resolution of the existing river routing model provides

measurable improvements, but resolution enhancement alone is insufficient to substantially eliminate systematic errors in ocean circulation and SST. The stronger and more spatially coherent improvements obtained in HALFv further demonstrate that routing parameters need to be appropriately calibrated when river resolution is changed, rather than simply transferring parameter values from a coarser configuration. More importantly, the systematic oceanic responses identified in both East Asian coastal waters and the tropical oceans demonstrate that river discharge represents a non-negligible component of the coupled climate system and can influence seasonal prediction through freshwater-induced changes in salinity, stratification, and circulation. These findings highlight the need to move beyond simple resolution enhancement toward a more sophisticated and physically realistic representation of river routing, including resolution-dependent parameter optimization and potentially additional hydrological processes. Further development of the river routing component could therefore provide an important pathway for improving the representation of ocean circulation and SST in future operational coupled seasonal prediction systems.

Several limitations of this study should be acknowledged. The experiments were conducted over a relatively limited period, and the higher-resolution configurations retained the fundamental structure and physical processes of the existing TRIP model. Therefore, increasing spatial resolution alone cannot fully address biases arising from missing or simplified hydrological processes. Longer-term hindcast experiments are currently being conducted with the latest version of the GloSea system, which will allow the robustness of the impacts identified here to be evaluated more comprehensively. Furthermore, the ongoing development of a new seasonal prediction system provides an opportunity to incorporate a more sophisticated river routing scheme. The systematic

oceanic responses identified in this study nevertheless demonstrate that the representation of river discharge is relevant to the simulation of ocean circulation and SST, highlighting the need to move beyond simple resolution enhancement toward a more physically realistic treatment of river processes in future coupled seasonal prediction systems.

Acknowledgments

This research was funded by the Korea Meteorological Administration Research and Development Program “APEC Climate Center for Climate Information Services” under Grant KMA2013-03410. This work was tested on KISTI/KREONET. Authors from KMA were funded by the Korea Meteorological Administration Research and Development Program “Operating and Developing Global Seasonal Forecast System (KMA2018-00320)”. Experiments in this studies were conducted using a supercomputer provided by the National Center for Meteorological Supercomputer at KMA.

Author contributions

All authors contributed to the conception and design of this study. Material preparation, data collection, and modification of TRIP codes were performed by Suryun Ham, Johan Lee, and Beomcheol Shin. The first draft of the manuscript was written by Suryun Ham and all authors commented on previous versions of the manuscript. All the authors have read and approved the final version of the manuscript.

Funding

The authors have not disclosed any funding.

Data availability

The datasets analyzed during the current study are not publicly available because of network issues but are available from the corresponding author upon reasonable request.

Declaration

Conflict of interests

The authors have no relevant financial or non-financial interests to disclose.

References

Alfieri, L., P. Burek, E. Dutra, B. Krzeminski, D. Muraro, J. Thielen, and F. Pappenberger, 2013: GloFAS—Global ensemble streamflow forecasting and flood early warning. *Hydrol. Earth Syst. Sci.*, **17**, 1161–1175, https://doi.org/10.5194/hess-17-1161-2013.

Boussetta, S., and Coauthors, 2021: ECLand: The ECMWF land surface modelling system. *Atmosphere*, **12**, 723, https://doi.org/10.3390/atmos12060723.

Burek, P., J. van der Knijff, and A. de Roo, 2013: LISFLOOD—Distributed water balance and flood simulation model: Revised user manual 2013. Publications Office of the *European Union*, https://doi.org/10.2788/24719.

Falloon, P. D., and R. A. Betts, 2006: The impact of climate change on global river flow in HadGEM1 simulations. *Atmos. Sci. Lett.*, **7**, 62–68, https://doi.org/10.1002/asl.133.

Gudmundsson, L., and Coauthors, 2021: Globally observed trends in mean and extreme river flow attributed to climate change. *Science*, **371**, 1159–1162, https://doi.org/10.1126/science.aba3996.

Ham, S., S.-Y. Hong, Y. Noh, S.-I. An, Y.-H. Byun, H.-S. Kang, J. Lee, and W.-T. Kwon, 2012: Effects of freshwater runoff on a tropical Pacific climate in the HadGEM2. *Asia-Pac. J. Atmos. Sci.*, **48**, 457–463, https://doi.org/10.1007/s13143-012-0041-3.

Ham, S., Y. Jeong, J. H. Yoo, S. Lim, H. Ji, and Y.-K. Hyun, 2024: What is the effect of atmospheric initial condition inconsistency between the hindcasts and real-time forecasts? *Climate Dyn.*, **62**, 1613–1623, https://doi.org/10.1007/s00382-023-06972-8.

Hersbach, H., and Coauthors, 2020: The ERA5 global reanalysis. *Quart. J. Roy. Meteor. Soc.*, **146**, 1999–2049, https://doi.org/10.1002/qj.3803.

Hirpa, F. A., P. Salamon, H. E. Beck, V. Lorini, L. Alfieri, E. Zsoter, and S. J. Dadson, 2018: Calibration of the Global Flood Awareness System (GloFAS) using daily streamflow data. *J. Hydrol.*, **566**, 595–606, https://doi.org/10.1016/j.jhydrol.2018.09.052.

Howden, S. D., and R. Murtugudde, 2001: Effects of river inputs into the Bay of Bengal. *J. Geophys. Res.*, **106**, 19 825–19 843, https://doi.org/10.1029/2000JC000656.

Kako, S., T. Nakagawa, K. Takayama, N. Hirose, and A. Isobe, 2016: Impact of Changjiang River discharge on sea surface temperature in the East China Sea. *J. Phys. Oceanogr.*, **46**, 1735–1750, https://doi.org/10.1175/JPO-D-15-0167.1.

Kettleborough, J. A., P. J. Davis, R. E. Comer, M. J. Martin, A. Barbosa Aguiar, T. Collier, A. A. Scaife, A. Clark, J. Mancell, K. A. Smout-Day, and S. C. Hardiman, 2025: Global Seasonal Forecasting System 6 (GloSea6): A Large Ensemble Seasonal Forecasting System. *Mon. Wea. Rev.*, **154**, 39–57. https://doi.org/10.1175/MWR-D-25-0007.1.

Kim, M., U.-Y. Byun, E.-C. Chang, and Y.-J. Lim, 2025: Impact of spatial resolution on river flow simulation based on the Total Runoff Integrating Pathway (TRIP) model. *Atmosphere*, **16**, 1083, https://doi.org/10.3390/atmos16091083.

Lee, S.-W., D. Lee, S. Noh, G.-U. Kim, and Coauthors, 2025: Sequential evolution of Changjiang Diluted Water and its impact on stratification and phytoplankton blooms in the East China Sea during summer 2020. *J. Geophys. Res. Oceans*, **130**, e2025JC022655, https://doi.org/10.1029/2025JC022655.

Li, H., Z. Zhang, and Z. Zhang, 2024: Improvement and evaluation of CLM5 application in the Songhua River Basin based on CaMa-Flood. *Water*, **16**, 442, https://doi.org/10.3390/w16030442.

MacLachlan, C., and Coauthors, 2015: Global Seasonal forecast system version 5 (GloSea5): A high-resolution seasonal forecast system. *Quart. J. Roy. Meteor. Soc.*, **141**, 1072–1084, https://doi.org/10.1002/qj.2396.

Masson, S., and P. Delecluse, 2001: Influence of the Amazon River runoff on the tropical Atlantic. *Phys. Chem. Earth Part B*, **26**, 137–142.

Ngo-Duc, T., T. Oki, and S. Kanae, 2007: A variable streamflow velocity method for global river routing model: Model description and preliminary results. *Hydrol. Earth Syst. Sci. Discuss.*, **4**, 4389–4414, https://doi.org/10.5194/hessd-4-4389-2007.

Nitta, T., T. Arakawa, M. Hatono, A. Takeshima, and K. Yoshimura, 2020: Development of Integrated Land Simulator. *Prog. Earth Planet. Sci.*, **7**, 68, https://doi.org/10.1186/s40645-020-00383-7.

Oki, T., 1997: Validating the runoff from LSP-SVAT models using a global river routing network by one degree mesh. *In Proc. 13th Conf. on Hydrology*, 319-322, Amer. Meteor. Soc.

Oki, T., and Y. C. Sud, 1998: Design of Total Runoff Integrating Pathways (TRIP)—A global river channel network. *Earth Interaction 2*, 1–37.

Pappenberger, F., H. L. Cloke, G. Balsamo, T. Ngo-Duc, and T. Oki, 2010: Global runoff routing with the hydrological component of the ECMWF NWP system. *Int. J. Climatol.*, **30**, 2155–2174, https://doi.org/10.1002/joc.2028.

584 Park, T., C. J. Jang, J. H. Jungclaus, H. Haak, W. Park, and I. S. Oh, 2011: Effects of the
585 Changjiang River discharge on sea surface warming in the Yellow and East China
586 Seas in summer. *Cont. Shelf Res.*, **31**, 15–22,
587 https://doi.org/10.1016/j.csr.2010.10.012.
588 Sanchez, C., K. D. Williams, and M. Collins, 2016: Improved stochastic physics
589 schemes for global weather and climate models. *Quart. J. Roy. Meteor. Soc.*, **142**,
590 147–159, https://doi.org/10.1002/qj.2640.
591 Sauer, I. J., R. Reese, C. Otto, T. Geiger, S. N. Willner, B. P. Guillod, D. N. Bresch, and
592 K. Frieler, 2021: Climate signals in river flood damages emerge under sound
593 regional disaggregation. *Nature Communications*, **12**, 2128,
594 https://doi.org/10.1038/s41467-021-22153-9.
595 Tennant, W. J., G. J. Shutts, A. Arribas, and S. A. Thompson, 2011: Using a stochastic
596 kinetic energy backscatter scheme to improve MOGREPS probabilistic forecast
597 skill. *Mon. Wea. Rev.*, **139**, 1190–1206, https://doi.org/10.1175/2010MWR3430.1.
598 Walters, D., and Coauthors, 2017: The Met Office Unified Model Global Atmosphere
599 6.0/6.1 and JULES Global Land 6.0/6.1 configurations. *Geosci. Model Dev.*, **10**,
600 1487–1520, https://doi.org/10.5194/gmd-10-1487-2017.
601 Williams, K. D., and Coauthors, 2015: The Met Office Global Coupled model 2.0 (GC2)
602 configuration. *Geosci. Model Dev.*, **8**, 1509–1524, https://doi.org/10.5194/gmd-8-
603 1509-2015.
604 Woldemeskel, F., and Coauthors, 2025: Assessment of JULES land surface model
605 coupled with CaMa-Flood for an operational streamflow forecasting across
606 Australia. *Hydrol. Processes*, **39**, e70345, https://doi.org/10.1002/hyp.70345.

607 Zhang, L., L. Wu, and J. Zhang, 2011: Simulated response to recent freshwater flux
608 change over the Gulf Stream and its extension: Coupled ocean–atmosphere
609 adjustment and Atlantic–Pacific teleconnection. *J. Climate*, **24**, 3971–3988,
610 https://doi.org/10.1175/2011JCLI4020.1.
611 Zuo, H., M. A. Balmaseda, S. Tietsche, K. Mogensen, and M. Mayer, 2019: The
612 ECMWF operational ensemble reanalysis–analysis system for ocean and sea ice:
613 A description of the system and assessment. *Ocean Sci.*, **15**, 779–808,
614 https://doi.org/10.5194/os-15-779-2019.
615

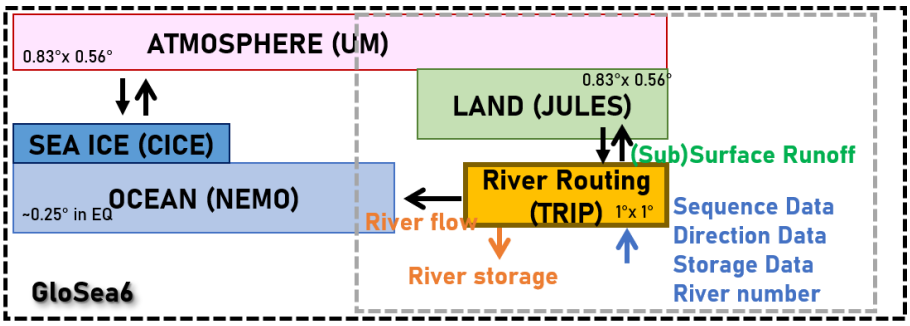


Fig. 1. Schematic diagram of GloSea6 showing the component models, their spatial resolutions, and the input and output variables associated with the river-routing model.

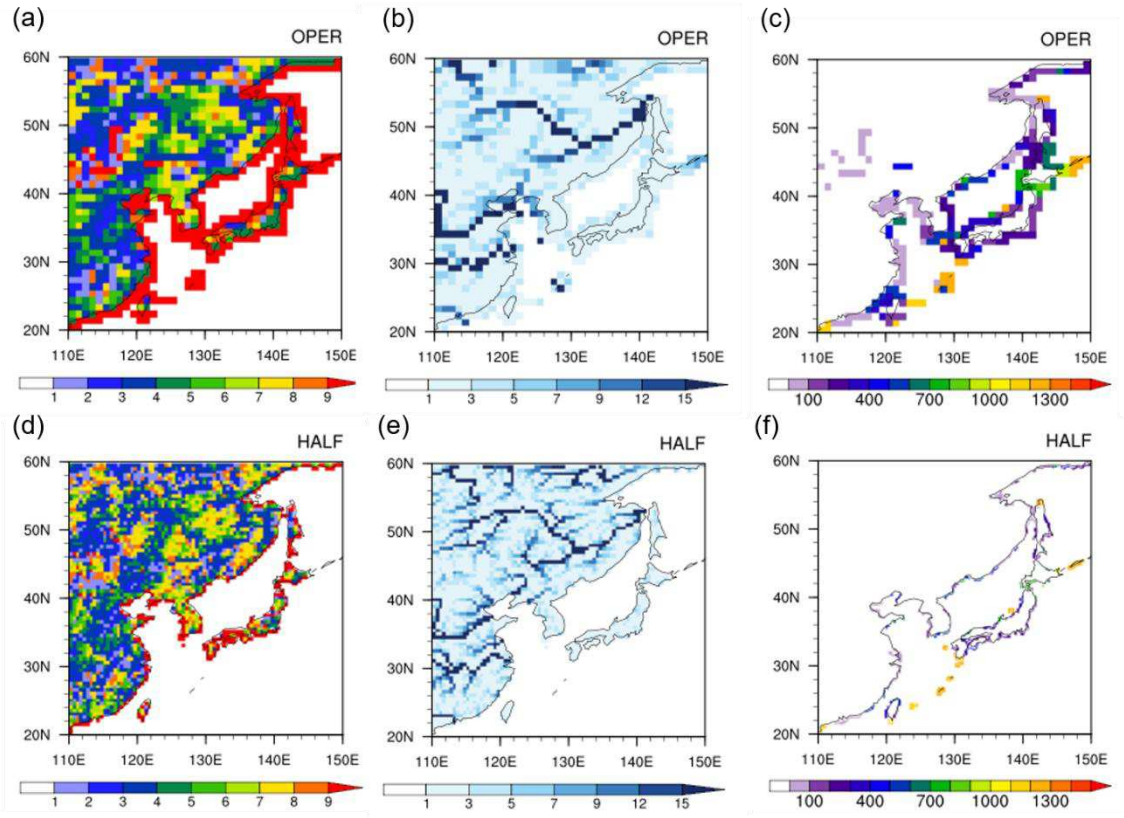


Fig. 2. GloSea6 ancillary datasets for (a-c) OPER and (d-f) HALF: (a, d) river direction, (b, e) river sequence, and (c, f) river-number maps.

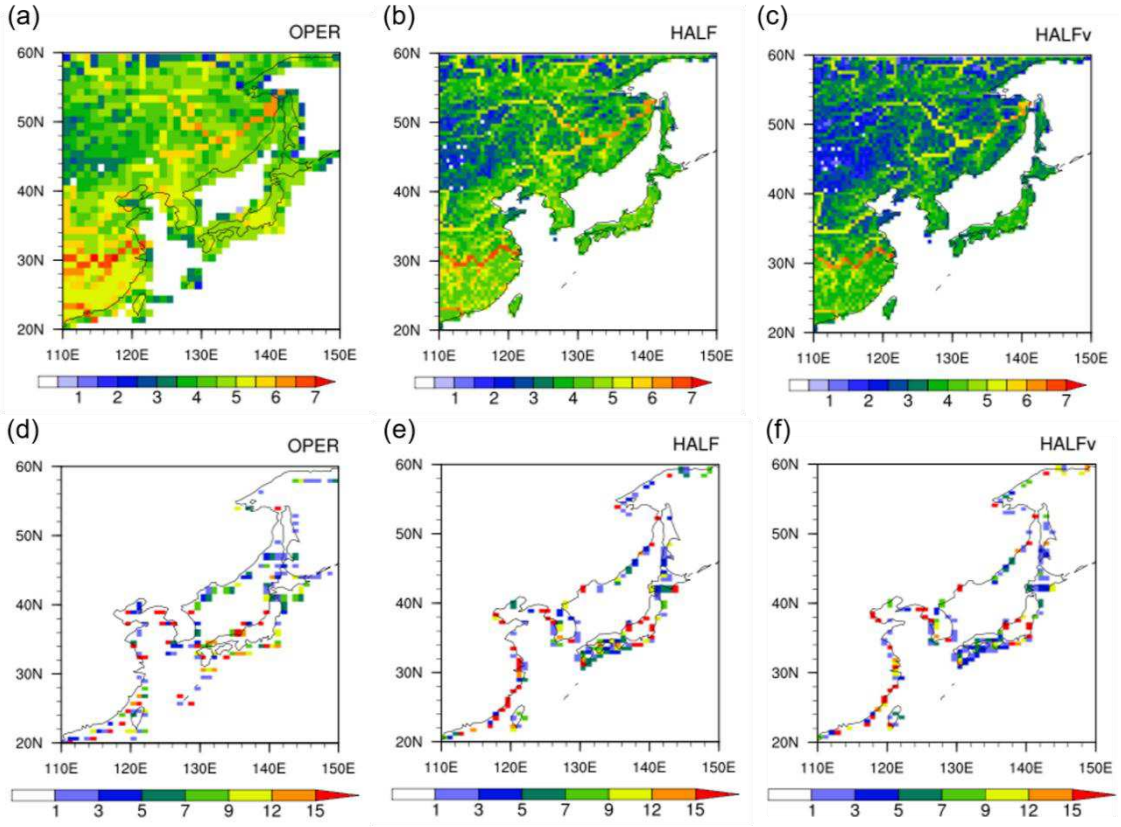


Fig. 3. Spatial distributions of (a-c) river water storage ($\log_{10}$ kg s^{-1}), and (d-f) river outflow (kg m^{-2}) for the OPER, HALF, and HALFv experiments, respectively.

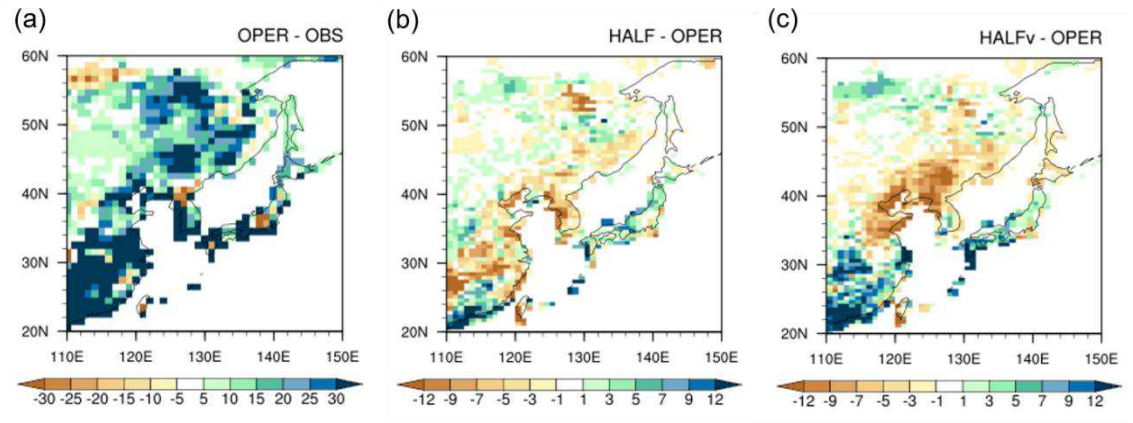


Fig. 4. Surface runoff (mm month^{-1}) for (a) the OPER bias relative to ERA5, (b) difference between the HALF and OPER, and (c) difference between the HALFv and OPER.

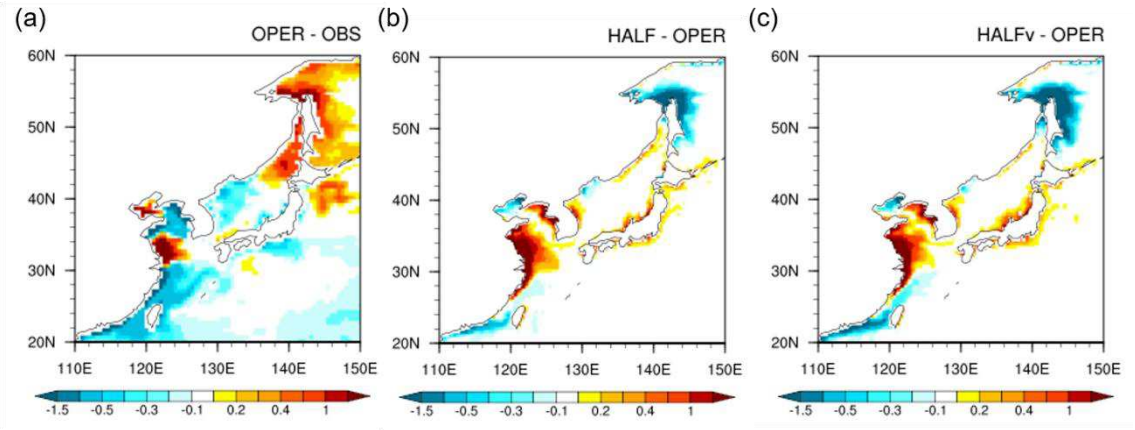


Fig. 5. Same as Fig. 4, but for sea surface salinity (psu).

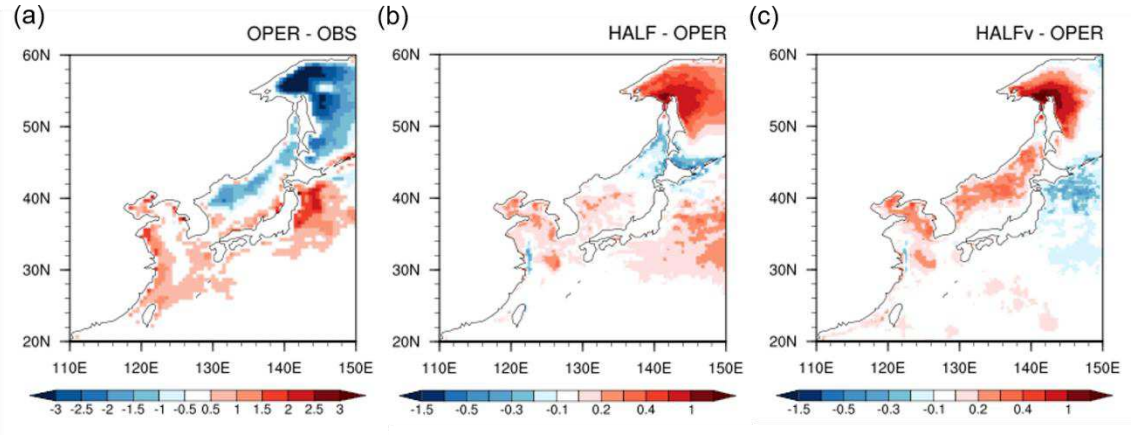


Fig. 6. Same as Fig. 4, but for sea surface temperature (˚C).

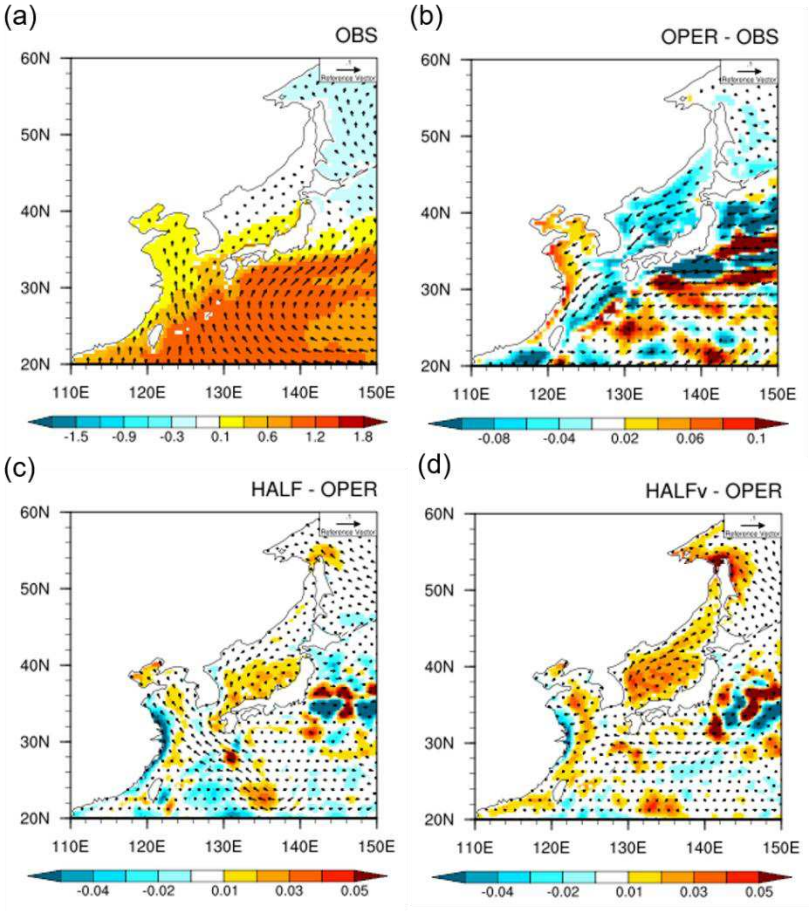


Fig. 7. Sea surface height(shading) and surface stress(vector) for (a) ORAS5, (b) the OPER bias relative to ORAS5, (c) the HALF minus OPER difference, and (d) the HALFv minus OPER difference.

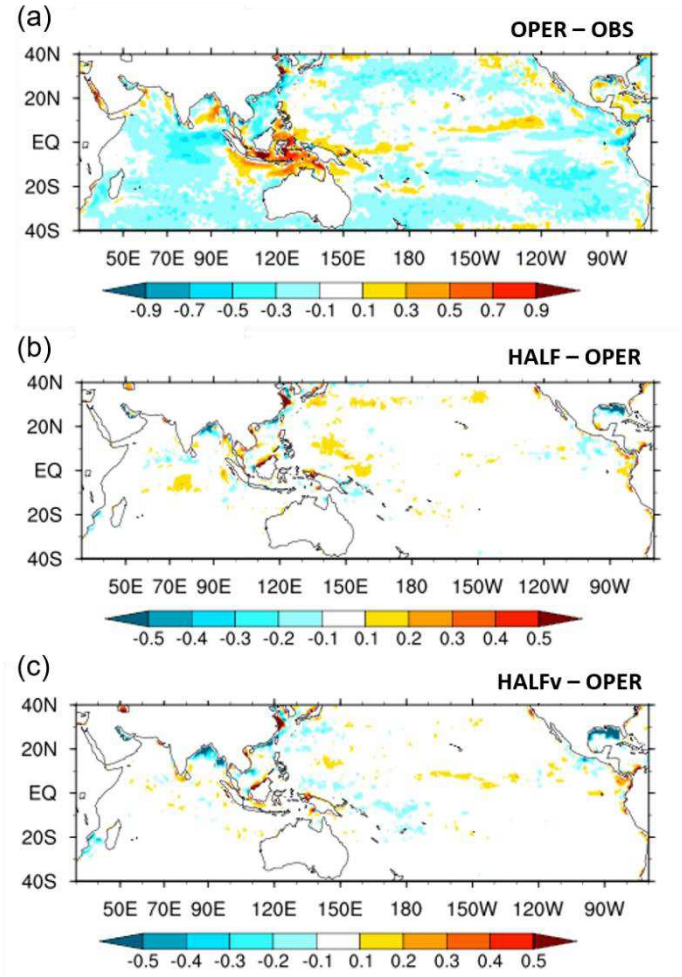


Fig. 8. Same as Fig. 5, but for the broader Indo-Pacific domain.

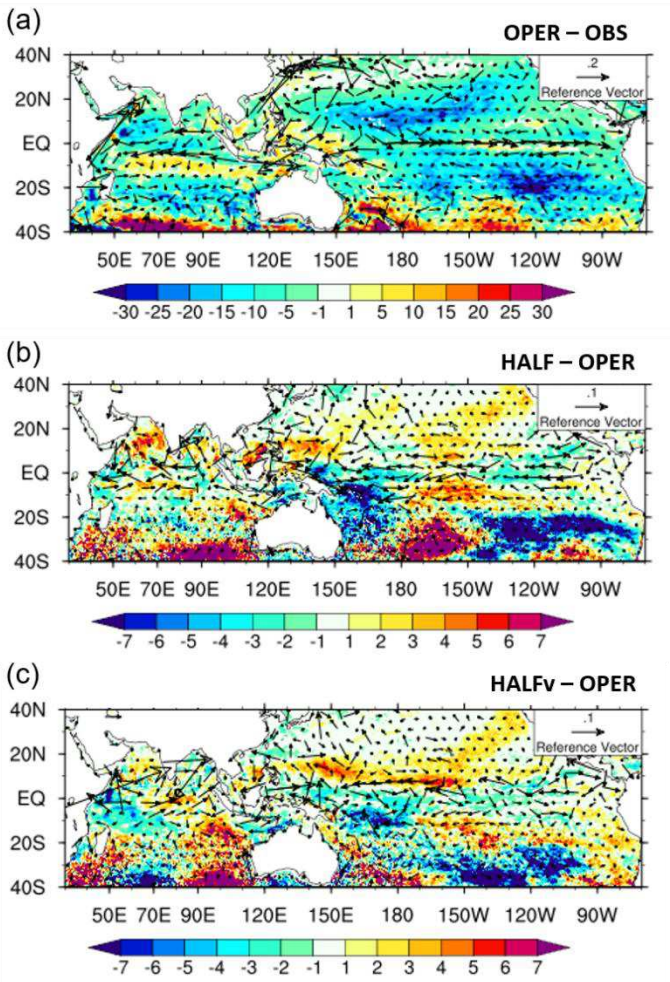


Fig. 9. Mixed layer depth (shading) and ocean current (vector) for (a) the OPER bias relative to ORAS5, (b) the HALF minus OPER difference, and (c) the HALFv minus OPER difference.

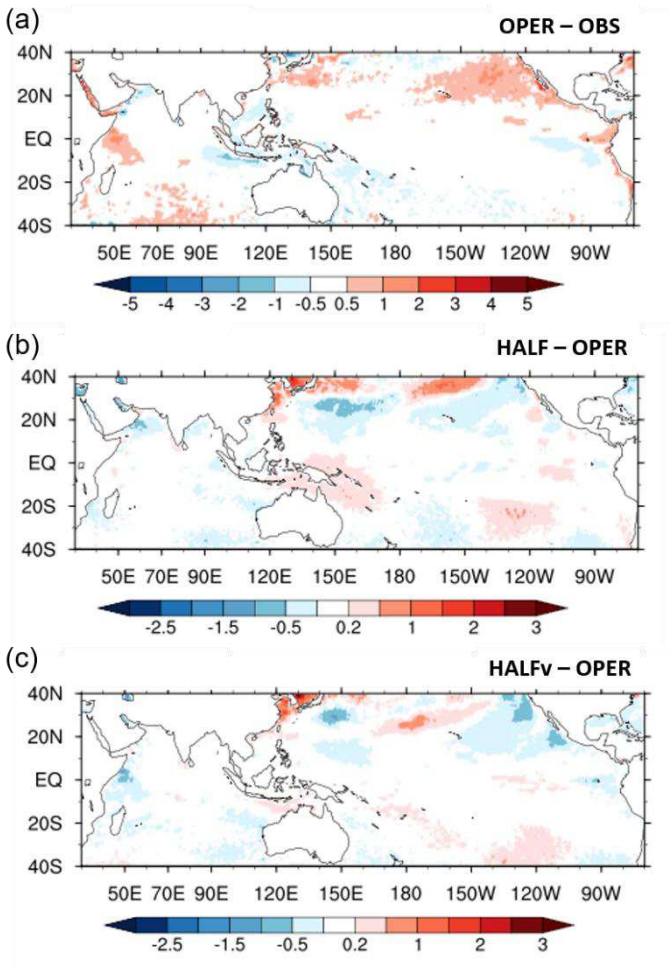


Fig. 10. Same as Fig. 8, but for sea surface temperature (˚C).

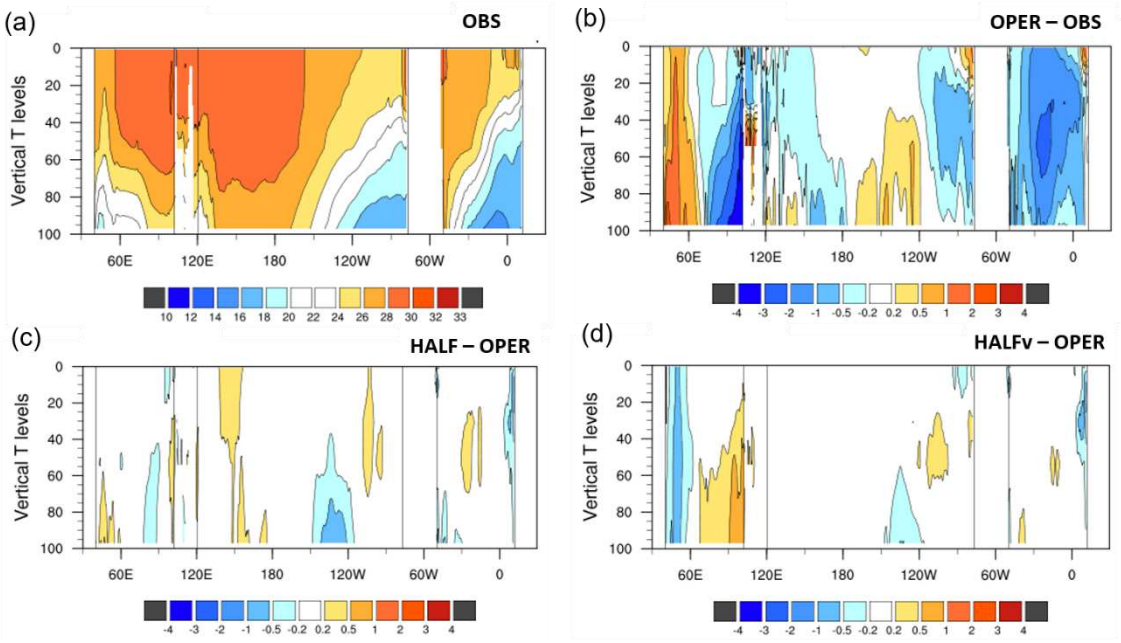


Fig. 11. Vertical ocean temperature (°C) averaged over 5°S-5°N for (a) ORAS5, (b) the OPER bias relative to ORAS5, (c) the HALF minus OPER difference, and (d) the HALFv minus OPER difference.